Study of the impedance mismatch at the output end of a THz parallel-plate waveguide

Marx Mbonye, Rajind Mendis,[a] and Daniel M. Mittleman
Department of Electrical and Computer Engineering, Rice University, MS 378, Houston, Texas 77251, USA

(Received 28 August 2011; accepted 1 March 2012; published online 16 March 2012)

We study the reflection of terahertz (THz) radiation at the end of a parallel-plate waveguide (PPWG), due to the impedance mismatch between the propagating transverse-electromagnetic mode and the free-space background. We find that, for a PPWG with uniformly spaced plates, the reflection coefficient at the output face increases as the plate separation decreases, consistent with predictions by early low frequency ray optical theory. We also study the reflection coefficient for tapered PPWGs where the plate spacing is tapered, for which no analytical theory exists, and quantify the reflection coefficient as a function of the plate separation and the THz frequency. © *2012 American Institute of Physics*. [http://dx.doi.org/10.1063/1.3695329]

Since it was first observed that a parallel-plate waveguide (PPWG) could support undistorted propagation of terahertz (THz) pulses via its dominant transverse electromagnetic (TEM) mode,[1] the PPWG has been exploited for a plethora of THz applications. These include spectroscopy,[2,3], imaging,[4] sensing,[5] and many others.[6–9] Very recently, tapered PPWGs have been used for achieving subwavelength confinement of THz radiation (even super-focusing) over a broad spectral bandwidth[10–12] with potential applications in near-field imaging and spectroscopy of subwavelength materials. For nearly, all of these applications, it is important to have a good understanding of the impedance mismatch between the propagating mode and the free space background, since this could influence the transmission throughput of the device. For example, a strong frequency dependence in this impedance mismatch may lead to significant distortions of the time-domain THz pulse, which could complicate the interpretation of near-field measurements. However, for the important case of a tapered PPWG and even for most implementations of a conventional (untapered) PPWG, there is no simple analytical theory which is valid in the regime of $b \sim \lambda$ or $b < \lambda$, where b is the plate separation.

In this work, we study the impedance mismatch between the propagating TEM wave in the PPWG and the free space background, at the output face of the abruptly terminated waveguide. This mismatch results in a fraction of the propagating wave being reflected at the output facet, back into the waveguide. We quantify the impedance mismatch by measuring this back-reflected wave after it emerges from the input end of the waveguide. We study both uniformly spaced and tapered waveguides, and compare to the existing theoretical treatments.

A schematic of the experimental setup is shown in Fig. 1. We use two synchronized mode-locked erbium-doped fiber lasers in an electronically controlled optical sampling (ECOPS) configuration.[13,14] THz pulses are generated via surface emission from a bare p-InAs wafer, and these pulses are detected using a LT-GaAs photoconductive antenna, gated with the second harmonic of the probe laser. The THz radiation is guided using a polyethyelene lens through a thin silicon beam splitter. A cylindrical teflon lens is used to focus the THz beam into the waveguide to excite the TEM mode. A metal mirror can be placed at the output face of the waveguide to retro-reflect the guided mode back towards the input facet, or it can be removed to allow the THz pulse to emerge from the waveguide into free space. In this way, we can compare the incident pulse propagating in the waveguide (measured by retro-reflection from the metal mirror) to the pulse reflected due to the impedance mismatch between the guided wave and free space (as measured when the retro-reflector is absent).

We compare the THz pulses measured with and without the retro-reflecting mirror, for several different plate separations, for a waveguide length of $L = 12.7$ mm. Results, for $b = 1.8$ mm, 1 mm, and 0.63 mm, are plotted in Figs. 2(a)–2(c). In these figures, the reflection from the front facet of the waveguide arrives earlier in time followed by the reflection from the back of the waveguide. The feature (12 ps) immediately following the initial THz pulse and the one following

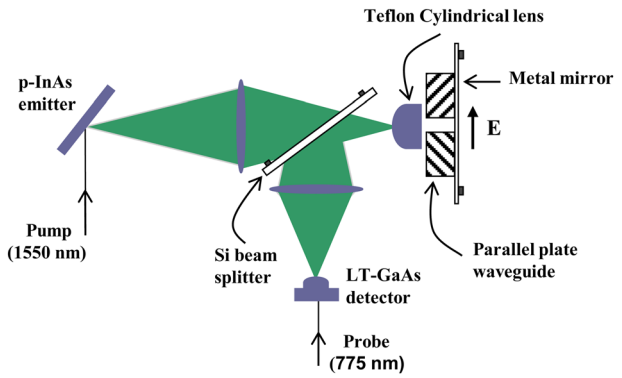

FIG. 1. (Color online) Schematic of the experimental setup. THz pulses from a bare p-InAs wafer are focused into the waveguide with the right polarization to excite the TEM mode. A metal mirror can be placed at the output face of the waveguide to retro-reflect the TEM mode, or it can be removed to allow the THz pulse to emerge from the waveguide into free space. A silicon beam splitter directs the retro-reflected signal to a LT-GaAs receiver for coherent detection.

[a]Author to whom correspondence should be addressed. Electronic mail: rajind@rice.edu.

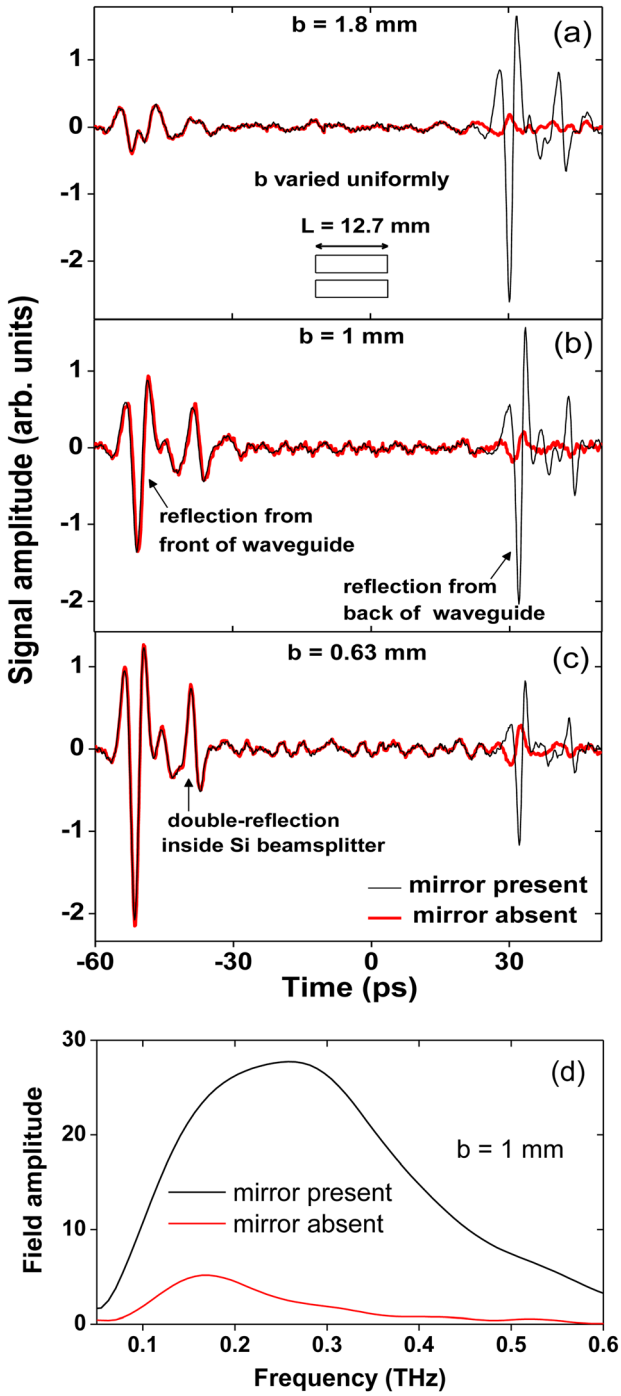

FIG. 2. (Color online) THz pulses measured with and without the retro-reflecting mirror, for a 12.7 mm long waveguide with three different plate separations: (a) $b = 1.8$ mm, (b) $b = 1$ mm, and (c) $b = 0.63$ mm. The reflection from the front end of the waveguide arrives earlier in time followed by the reflection from the back end of the waveguide. The feature (12 ps) immediately following the initial THz pulse and the one following the pulse reflected from the back end of the waveguide are due to multiple reflections inside the silicon beam splitter. Amplitude spectra corresponding to the relevant reflections for $b = 1$ mm are shown in (d).

the pulse reflected from the back of the waveguide are due to multiple reflections inside the silicon beam splitter. In each case, the signals arising from reflections at the front face of the waveguide are unchanged by the removal of the retro-reflecting mirror, as expected. However, the reflection originating from the back facet of the waveguide, at a later delay, changes dramatically when this mirror is removed, exhibiting a diminished amplitude and a reversed polarity. By comparing these two reflections (with and without the retro-reflecting mirror), we can estimate the impedance mismatch (or reflection coefficient) between the guided wave and free space. This reflection coefficient is expressed as the ratio between the signal with the reflector absent and the signal when it is present.

Fig. 3 shows the measured amplitude reflection coefficient for a 12.7 mm long waveguide when the plate separation is varied uniformly. The width of the waveguide is chosen to be sufficiently larger (25.4 mm in size) than the input beam diameter, so that the waveguide mimics *infinitely wide* plates to the propagating beam. Therefore, the width has no bearing on the results. The reflection coefficients are obtained from the Fourier transforms of the relevant truncated portions of the measured time-domain waveforms. The Fourier-transformed amplitude spectra corresponding to $b = 1$ mm are shown in Fig. 2(d). In Fig. 3, we note that, for large plate separations, most of the propagating wave is transmitted into empty space and is not reflected back to the detector, and therefore, the reflection coefficient increases as the plate separation decreases. Additionally, for a given plate separation, the reflection coefficient increases as the wavelength increases.

Fig. 4 shows logarithmic plots of the reflection coefficient for the TEM mode versus the ratio of the plate separation to the wavelength (b/λ). The experimental data points in Figs. 4(a) and 4(b) correspond to 170 GHz and 300 GHz, respectively, and are for two waveguides with $L = 12.7$ mm and 25.4 mm. These are plotted along with approximate results predicted by ray optical theory.[15,16] Exact results are only available for the case where the waveguide plates are infinitely thin.[17,18] Following the analysis in Ref. 15, for our case, where the plates have a finite thickness, the ray optical theory considers the input beam to consist of two plane waves: one traveling along and almost parallel to the top plate and the other propagating in the same manner along the bottom plate. Once the plane waves reach the end of the waveguide, they are "scattered" back after diffraction from the edges at the output end of the waveguide. The reflection

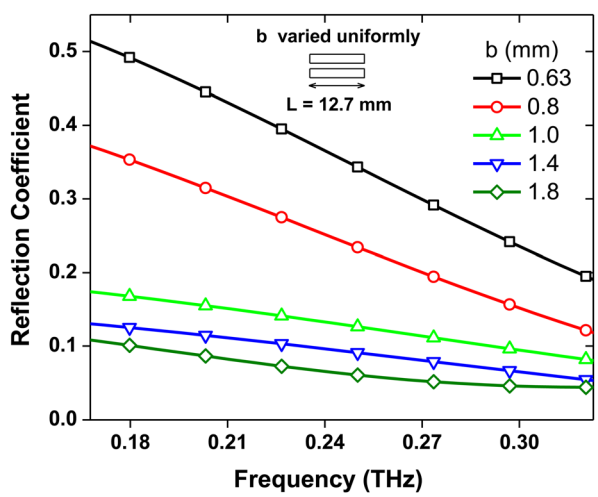

FIG. 3. (Color online) Measured amplitude reflection coefficient for a 12.7 mm long PPWG, for several different plate separations. Here, the plate separation is uniform along the direction of propagation.

coefficient is derived based on the resultant sum of these diffracted waves. The inset in Fig. 4(b) shows the two waves u and $\bar{u}$ (symbols denoting normalized amplitudes) that are scattered by the lower and upper edges, respectively. Equations (1) and (2) describe the reflection coefficient for a particular TM mode assuming only primary diffraction, where higher-order diffraction that results from multiple interactions at the output edges has been ignored,

$$\Gamma_{Nn} = [(-1)^n u D(\alpha, \theta_n, \theta_N) + \bar{u} D(\alpha, \theta_n, \theta_N)] \frac{\sqrt{2\pi k}}{2K_n b} e^{i\pi/4}, \tag{1}$$

$$D(\alpha, \phi, \theta_N) = \frac{e^{i\pi/4}}{2\sqrt{2\pi k}} \left\{ -\frac{2\pi}{\alpha} \sin\frac{\pi^2}{\alpha} \left[\frac{1}{\cos\pi(\phi - \theta_N)/\alpha - \cos\pi^2/\alpha} + \frac{1}{\cos\pi(\phi + \theta_N)/\alpha - \cos\pi^2/\alpha} \right] \right\}. \tag{2}$$

Here, Γ_{Nn} is the reflection coefficient corresponding to the nth mode due an incident Nth mode, θ is the incidence angle of the decomposed waves, α is the exterior wedge angle (at the output edges), and K_n is the phase constant of the nth mode.

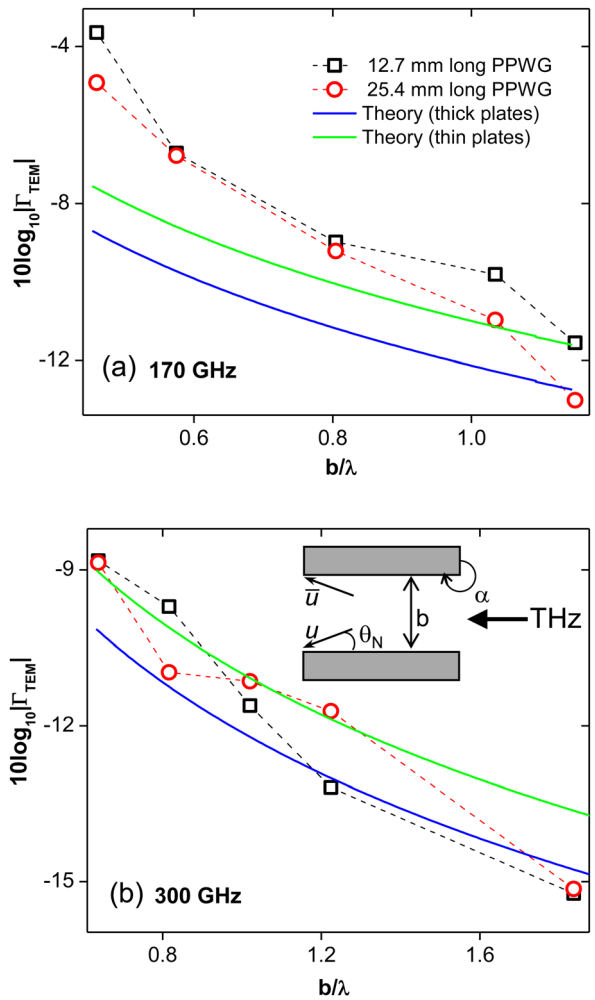

FIG. 4. (Color online) Logarithmic plots of the amplitude reflection coefficient for the TEM mode. The black squares and red circles correspond to measured values for a 12.7 mm long and a 25.4 mm long waveguide, respectively. The solid blue and green curves correspond to the calculated values using ray optical theory for thick and infinitely thin plates, respectively. Parts (a) and (b) correspond to the frequencies of 170 GHz and 300 GHz, respectively, at which the experimental points were derived (from Fig. 3, for example). The inset in (b) shows a schematic used for the calculation.

For our case, where propagation is purely due to the dominant TEM mode, $n = 0$, $\theta_n = \theta_N = 0$, $\alpha = \frac{3}{2}\pi$, $k = K_n = \frac{2\pi}{\lambda}$, and $u = \bar{u} = \frac{1}{2}$. Combining Eqs. (1) and (2) with these substitutions, we can derive the magnitude of the reflection coefficient for the single-TEM mode as

$$|\Gamma_{TEM}| = 0.0613\left(\frac{\lambda}{b}\right). \tag{3}$$

Equation (3), although approximate, implies an (inversely) linear b/λ dependence. The corresponding theoretical curves [solid blue curves in Figs. 4(a) and 4(b)] show reasonable agreement with the experimental results. Additionally, we have shown theoretical curves corresponding to infinitely thin plates [solid green curves in Figs. 4(a) and 4(b)], which indicate the same dependence but with a slightly higher overall magnitude. The lower magnitude in the case of thick plates is probably caused by the softening of the physical discontinuity due to the 90° edge at the output end.

In order to achieve smaller plate separations than were possible with the uniformly spaced PPWG, next, we resort to a tapered PPWG. At smaller plate separations, the significantly reduced energy coupling into the uniformly spaced

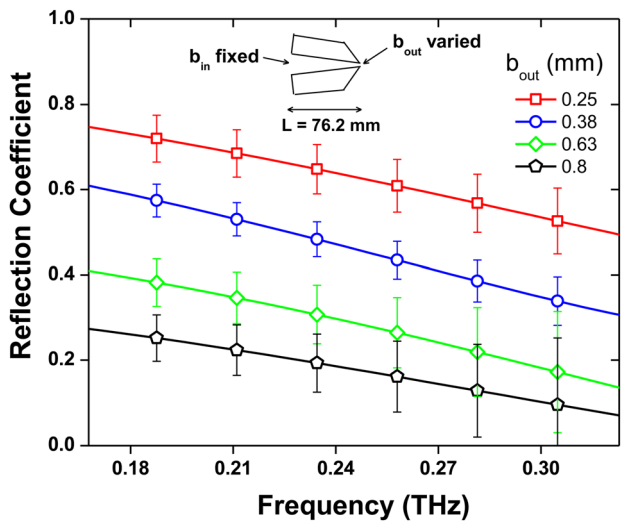

FIG. 5. (Color online) Measured amplitude reflection coefficient for a 76.2 mm long tapered PPWG with a knife-edged output end. An axial cross-section of this waveguide is shown in the inset.

waveguide would preclude a reliable measurement. However, using a tapered waveguide, the input plate spacing could be held constant at a sufficiently large size to couple enough energy, while the output plate spacing is varied. An axial cross-section of this tapered waveguide is shown in the inset of Fig. 5, whose output ends are formed into knife edges. This knife-edge geometry permits us to place the retro-reflecting mirror very close to the output aperture even for the largest taper angle, which is crucial for obtaining an accurate measurement of the reference waveform. For these measurements, the plate separation of the waveguide at the input facet is kept fixed at 2.3 mm, using steel ball-bearings as spacers to provide sufficient pivoting for the surfaces of the plates. Only the output plate separation of the waveguide is varied.

As before, the reflection coefficient is derived after Fourier transforming the relevant portions of the time domain data. Similar to the previous case (with uniformly spaced plates), the reflection coefficient is found to increase as the output plate spacing is decreased (for a given frequency) and also when the frequency is decreased (for a given output plate separation). This latter dependence has also been observed in a *finite-width* tapered PPWG very recently,[19] using an air-photonic field imaging technique. It should be noted that, in our data analysis, we are assuming that the forward propagating wave is not affected by the placement of the mirror in deriving the incident (reference) signal. This assumption is reasonable for large plate separations, but may not be quite valid at very small plate separations, where plasmonic effects dominate.[11] This probably explains the relatively higher estimated values for the reflection coefficient at smaller separations in Fig. 5, compared to what one might expect intuitively under TEM mode propagation.

Furthermore, since we are using an *adiabatic* taper, we can assume that there are no additional reflections due to the continuously varying local impedance in the tapered waveguide. The only appreciable reflection is caused by the abrupt impedance change at the output face. This implies that the reflection coefficients corresponding to both untapered and tapered waveguides having the same output plate separations, should match favorably. In fact, if we compare the curves for 0.63 mm and 0.8 mm in Figs. 3 and 5, we see that the differences are small and within experimental error.

In summary, we have characterized the impedance mismatch relevant for the dominant TEM mode of THz PPWGs. In the case of a PPWG with uniformly spaced plates, the reflection coefficient at the output-facet of the PPWG increases as the plate separation decreases. This dependence is approximately linear with the ratio b/λ, as predicted by a ray optical theory. This same trend is observed in tapered PPWGs, when the input separation is fixed and the output separation is varied. The reflection coefficients that we measure, especially for the smaller plate separations, are unexpectedly high, since one would not generally associate a high impedance mismatch under TEM mode propagation. These results shed more light on the propagation of THz radiation in practical PPWGs.

[1]R. Mendis and D. Grischkowsky, Opt. Lett. **26**, 846 (2001).
[2]J. S. Melinger, N. Laman, S. S. Harsha, and D. Grischkowsky, Appl. Phys. Lett. **89**, 251110 (2006).
[3]N. Laman, S. S. Harsha, D. Grischkowsky, and J. S. Melinger, Biophys. J. **94**, 1010 (2008).
[4]M. M. Awad and R. A. Cheville, Appl. Phys. Lett. **86**, 221107 (2005).
[5]J. Zhang and D. Grischkowsky, Opt. Lett. **29**, 1617 (2004).
[6]R. Mendis and D. Grishkowsky, IEEE Microw. Wirel. Compon. Lett. **11**, 444 (2001).
[7]Z. Jian, J. Pearce, and D. M. Mittleman, Opt. Lett. **29**, 2067 (2004).
[8]H. Cao, R. A. Linke, and A. Nahata, Opt. Lett. **29**, 1751 (2004).
[9]S. S. Harsha, N. Laman, and D. Grischkowsky, Appl. Phys. Lett. **94**, 091118 (2009).
[10]A. Rusina, M. Durach, K. A. Nelson, and M. I. Stockman, Opt. Express **16**, 18576 (2008).
[11]H. Zhan, R. Mendis, and D. M. Mittleman, Opt. Express **18**, 9643 (2010).
[12]H. Zhan, R. Mendis, and D. M. Mittleman, J. Opt. Soc. Am. B **28**, 558 (2011).
[13]S. Kray, F. Spöler, T. Hellerer, and H. Kurz, Opt. Express **18**, 9976 (2010).
[14]J. Liu, M. Mbonye, R. Mendis, and D. M. Mittleman, in OSA Technical Digest of Conference on Lasers and Electro-Optics, San Jose, CA, May 2010.
[15]H. Y. Yee, L. B. Felsen, and J. B. Keller, SIAM J. Appl. Math. **16**, 268 (1968).
[16]R. Rudduck and L. Tsai, IEEE Trans. Antennas Propag. **16**, 83 (1968).
[17]L. A. Vainshtein, *Theory of diffraction and method of factorization* (Izd. Soviet Radio, Moscow, 1966).
[18]J. Boersma, SIAM J. Appl. Math. **29**, 164 (1975).
[19]K. Iwaszczuk, A. Andryieuski, A. Lavrinenko, X.-C. Zhang, and P. U. Jepsen, Appl. Phys. Lett. **99**, 071113 (2011).